Proceedings World Geothermal Congress 2005
Antalya, Turkey, 24-29 April 2005

System Integration of Various Geophysical Measurements for Reservoir Monitoring

Tsuneo Ishido, Kazunori Goko[2], Masaho Adachi[3], Junichi Ishizaki[4], Toshiyuki Tosha, Yuji Nishi, Mituhiko Sugihara, Shinichi Takakura, and Tsuneo Kikuchi

Reservoir Dynamics RG, Geological Survey of Japan, GREEN, AIST, Central 7, 1-1-1 Higashi, Tsukuba 305-8567, Japan

[2]Nittetsu Kagoshima Geothermal Co.

[3]Okuaizu Geothermal Co.

[4]Tohoku Electric Power Co., Inc.

E-mail address, ishido-t@aist.go.jp

Keywords: reservoir monitoring, microgravity, self-potential, electrical resistivity, history-matching

ABSTRACT

Since 2002, we have been carrying out a cooperative research program entitled "System Integration of Various Geophysical Measurements for Reservoir Monitoring"; involving both the Okuaizu and Ogiri geothermal fields in Japan. This continuing work carries forward a completed 1997-2002 NEDO/GSJ project on the application of various geophysical survey techniques to reservoir monitoring and modeling. To appraise the utility of reservoir monitoring by simultaneous continuous/repeat measurements of gravity, SP and electrical resistivity for history-matching of reservoir models, we performed numerical simulations based upon two types of hypothetical reservoir models and calculated changes in these geophysical observables on the ground surface caused by changing reservoir conditions. On the basis of these calculations, we discuss a combination of multi-geophysical measurements which can provide useful additional constraints for history-matching studies.

1. INTRODUCTION

Numerical models of geothermal reservoirs are never precise, owing to the problem of non-uniqueness. The difficulty increases as the amount of available relevant field data becomes smaller. If only a few facts are known about the reservoir, a variety of theoretical reservoir models may explain these known facts equally well, but yield very different predictions of future potential. As the amount of field data available increases, of course, these uncertainties diminish. Thus, as time goes on, the understanding of the reservoir improves and forecasts become more reliable. Typically, the data base upon which numerical reservoir models are constructed consists of (1) geophysical surveys of various types, usually performed prior to development, (2) geological interpretations of underground structure, (3) downhole pressure and temperature surveys in shut-in wells, (4) flowing downhole surveys in wells, and (5) pressure-transient test results.

Once exploitation begins in earnest, additional data become available, such as temporal trends in downhole flowing pressures and wellhead enthalpies. These latter data may be used in "history-matching" studies. Since the uncertainty in the predictions of numerical reservoir models is directly related to the amount of field data available against which the models can be tested, the addition of repeat geophysical survey data to the above list of pertinent field measurements is likely to improve the reliability of the forecasts. It is well known in this connection that repeat precision gravity surveying has considerable promise for appraising the volumetric properties of any proposed mathematical reservoir model (e.g., Ishido et al., 1995).

The application of improved geophysical and geochemical techniques to reservoir management was among the objectives of a geothermal R&D project ("*Development of Technology for Reservoir Mass and Heat Flow Characterization*") which was carried out by NEDO (the New Energy and Industrial Technology Development Organization) as a part of METI's New Sunshine Program from 1997 through 2002 (e.g., Horikoshi et al., 2001; Yamasawa et al., 2001). GSJ (the Geological Survey of Japan) carried out supporting basic research in cooperation with NEDO, pursuing the development of improved field survey techniques and associated modeling studies involving geophysical survey techniques and their application to reservoir performance monitoring. In addition to gravity monitoring, these techniques included repeat self-potential, resistivity, and seismic velocity surveys (Figure 1).

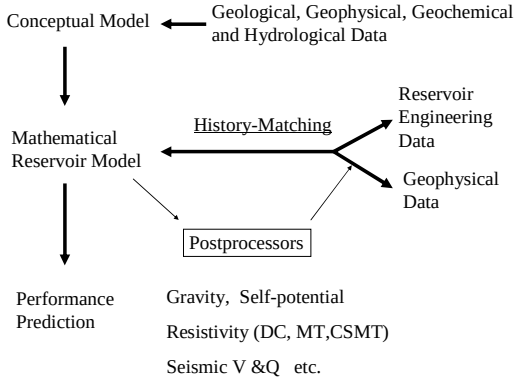

Figure 1: Geothermal reservoir modeling. Various computational postprocessors permit the user to calculate temporal changes that are likely to be observed if geophysical surveys of an operating geothermal field are repeated from time to time. Results may be used to supplement conventional reservoir engineering measurements in history-matching studies undertaken during geothermal reservoir model development.

In 2002, GSJ started a new cooperative research program, *"System Integration of Various Geophysical Measurements for Reservoir Monitoring"*, focused on the Okuaizu and Ogiri areas in Japan, to make practical applications of the

results of the NEDO/GSJ project. As a feasibility study, we performed numerical simulations based upon two types of hypothetical reservoir model to appraise reservoir monitoring by simultaneous continuous/repeat measurements of gravity, SP and other techniques for history-matching of reservoir models.

2. PREDICITON OF CHANGES IN GEOPHYSICAL OBSERVABLES

2.1 Illustrative Case I: High Temperature Fractured Reservoir

2.1.1 Reservoir Model

We consider the 3 km × 1.5 km × 2 km volume shown in Figure 2. The computational grid consists of 360 blocks (12 × 3 × 10). Four rock formations (*A*, *B*, *C* and *D*) are present, which differ in porosity and permeability. Other formation properties are uniform: rock grain density is 2600 kg/m^3, rock heat capacity is 1 kJ/kg-°C, and thermal conductivity is 2 W/m-°C. Relative permeabilities are simple straight-line functions with residual water and steam saturations of 30% and 5% respectively. The high-permeability reservoir (*A* in Fig. 2) is sandwiched by wall rocks (*D*) and overlain by the low-permeability altered caprock (*C*). At depth, a source of high-temperature (320°C)*"magmatic water"* (tagged with a dilute tracer) is imposed at the southeastern part of the bottom surface. The hot fluid recharges the reservoir and then flows outward toward the northwest through a less permeable formation (*B*). All vertical boundaries except a part of the northwestern surface are impermeable and insulated. Pressure and temperature are maintained at 30–40 bars and 80°C respectively along the top boundary (which is located at 0.5 km depth). Most of the bottom surface (at 2.5 km depth) is impermeable, but constant temperature (320°C) is imposed over the reservoir bottom surface. Any *"fresh water"* which flows downward into the grid through the top surface contains a dilute tracer to permit its identification. For the "EKP-postprocessor" calculations described in the next section, the *"magmatic"* and *"fresh"* waters are assumed to have NaCl concentrations of 0.3 and 0.017 mol/L respectively.

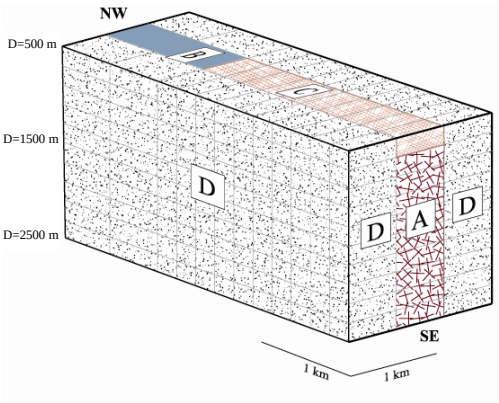

Figure 2: Three-dimensional hypothetical reservoir model for Case I. A high permeability reservoir (*A*) is sandwiched by wall rocks (D) and overlain by a cap rock (*C*). Deep natural hot water recharge is assumed at the southeastern ("SE") base of the reservoir. The hot fluid rises and leaves the reservoir to the northwest ("NW") through a less permeable formation (*B*).

We consider four variations of the above model: *"H-P"* (high *k*, porous), *"H-F"* (high *k*, fractured), *"L-P"* (low *k*, porous) and *"L-F"* (low *k*, fractured). Although all of these models have the same common features described above, the permeabilities of formations *A*, *B*, *C* and *D* and the rate of deep hot-fluid recharge for the *"L"* models are only one-tenth of those for the *"H"* models (for which the permeabilities are listed in Table 1 and the recharge rate is 40 kg/sec). Formation *A*, representing the reservoir, is assumed to be a "MINC" double-porosity medium (with fracture zone volume fraction ψ = 0.05, fracture zone porosity ϕ_f = 0.1, matrix region porosity ϕ_m = 0.1, matrix region permeability $k_m = 10^{-18}$ m^2, and fracture spacing λ = 30 m) for the *"F"* models, and is treated as equivalent porous medium for the *"P"* models.

Table 1: Rock porosities and permeabilities (*"H"* models) for Case I.

Formation	Porosity ϕ	Permeability (md) k_x	k_y	k_z
A (reservoir)	0.10	100.0	10.0	10.0
B	0.05	30.0	10.0	10.0
C (caprock)	0.05	0.1	0.1	0.1
D	0.05	3.0	3.0	3.0

The development of the hydrothermal convection system was computed for the *"H-P"* and *"L-P"* models using the STAR geothermal reservoir simulator (Pritchett, 1995). The system reached quasi-steady state after around 10,000 years of evolution (Figure 3). In the *"H-P"* model, a two-phase steam/water zone develops at shallow levels of the reservoir below the caprock.

The STAR simulator was next used to perform a 4-year forecast of the consequences of production, starting from the natural-states for the *"P"* models described above as the initial conditions. All boundary conditions and rock properties are the same as those used to calculate the natural-states. Fluid is withdrawn from six production wells at a fixed rate of ~100 tons/hour each (total rate of ~600

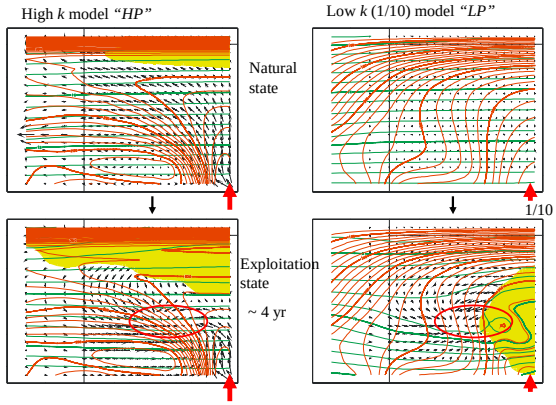

Figure 3: Distributions of temperature (contour interval 10°C), pressure (contour interval 10 bars), mass flux and the two-phase region (shaded area) under natural-state (upper) and exploited (lower) conditions for the *"H-P"* (left) and *"L-P"* (right) models. Feedpoints for six production wells are located within the ellipse.

tons/hour). No re-injection of waste fluid takes place in these calculations. Temperature, pressure, mass flux and the two-phase steam/water zone after ~4 years of field operation are shown in Figure 3 for the *"P"* models.

The temporal variations of reservoir pressure caused by field operation are shown in Fig. 3. In the calculations, the field is shut in for three months after ~1 and ~3 years of operation. As pressure decreases, the total volume occupied by steam in the reservoir increases from 0.6×10^7 m^3 under natural-state conditions to 2.2×10^7 and 1.3×10^7 m^3 after four years for the *"H-P"* and *"H-F"* models respectively, and from zero to 2.1×10^7 and 1.8×10^7 m^3 for the *"L-P"* and *"L-F"* models respectively. The produced fluid enthalpy is almost constant during the whole 4-year period except for the *"L-F"* model, which exhibits "excess enthalpy" after ~2 years of field operation.

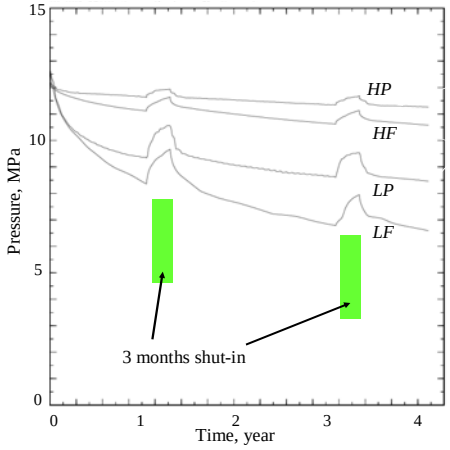

Figure 4: Pressure histories in an observation well located near the boundary between the *"A"* and *"B"* formations for the *"H-P"*, *"H-F"*, *"L-P"* and *"L-F"* models.

2.1.2 Changes in Microgravity and Self-Potential

Next, STAR's "gravity" and "EKP" postprocessors (see, e.g. Pritchett, 1995; Ishido and Pritchett, 1999; Ishido and Pritchett, 2003) were used to calculate the gravity and self-potential changes at the earth surface which are caused by changes in underground conditions that result from production. Figure 5 shows temporal changes in gravity and self-potential at a station located in the central production area.

The magnitude of gravity decrease is larger for the *"H-P"* model than that for the *"H-F"* model. This is because the total volume of steam created due to production-induced pressure decrease is larger for *"H-P"* than that for *"H-F"* as mentioned above. For the latter model, although the two-phase zone extends deeper and the vapor saturation (S_V) becomes very high in the fracture zone, S_V in the matrix region remains near zero for four years. The total volume of induced steam is similar for the *"L-P"* and *"L-F"* models and larger than for the *"H-P"* model (since the recharge from reservoir boundaries is negligible in the low permeability models). The intermediate magnitude of gravity decrease for the *"L"* models is due to the relatively deep location of the induced two-phase zone, as shown in Figure 3. For all four models, the rate of gravity decrease is reduced during the periods of field wide shut-in, but unlike pressure (Fig. 4) no actual recovery is seen.

Self-potential (SP) in the production area is positive under natural-state conditions and decreases rapidly after production begins for all models (Figure 5). Figure 6 shows a vertical section of the electrical potential distribution under natural-state conditions for the *"H"* models (the distribution for the *"L"* models is quite similar). Positive charge accumulates at shallow levels of the reservoir due to the high temperature upflow, which has less capacity to carry positive charge along the flow direction via electrokinetic coupling as temperature decreases (due to lower magnitude of the zeta potential; e.g., Ishido and Pritchett, 1999).

Exploitation drastically changes the SP distribution, as shown in Figure 7. Downward liquid flow in the production-induced boiling zone causes corresponding drag currents, resulting in negative potentials at shallower levels. Although a large subsurface positive potential appears associated with the production zone, it is confined within the region where pressure decreases in the cases of the *"H-P"* and *"H-F"* models. In both cases, the potential anomalies become quite weak by the end of the 3-month

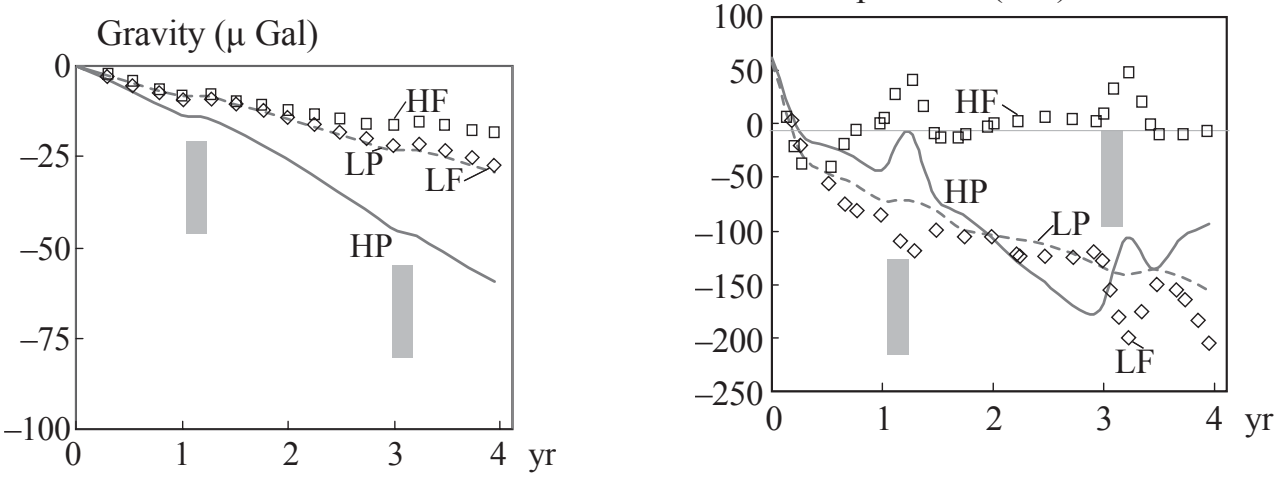

Figure 5: Changes in gravity and SP in the production area, calculated by applying the "mathematical postprocessors" to production-induced changes in reservoir conditions. In principle the *"H-P"*, *"H-F"*, *"L-P"* and *"L-F"* models can be distinguished based upon long- and short-term gravity and SP changes.

shut-in due to changing reservoir conditions (the bottom of two-phase zone moves upward with the shrinkage of the boiling zone, and the production zone pressure nearly recovers to the initial level). Because of the decreasing magnitude of the negative source, surface SP increases significantly during the shut-in as shown in Figure 5 (and actually becomes positive in the *"H-F"* case).

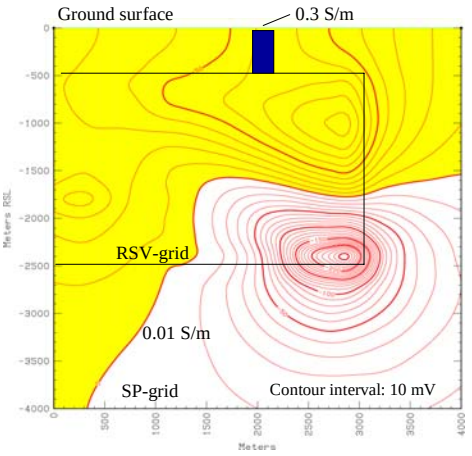

Figure 6: Cross-section of electric potential distribution under natural-state conditions for the *"H-P"* model. The reservoir simulation grid denoted as "RSV" is embedded in the "SP"-grid, which has a larger spatial extent than the "RSV"-grid. Within the portion of the "SP"-grid overlapped by the "RSV"-grid, the distribution of electrical conductivity is obtained directly from "RSV"-grid values. Elsewhere within the "SP"-grid, the electrical conductivity is assumed to be 0.01 S/m except the shaded zone between the ground surface and the top of "RSV"-grid (0.3 S/m). "EKP-postprocessor" calculation procedure is described by Ishido and Pritchett (1999).

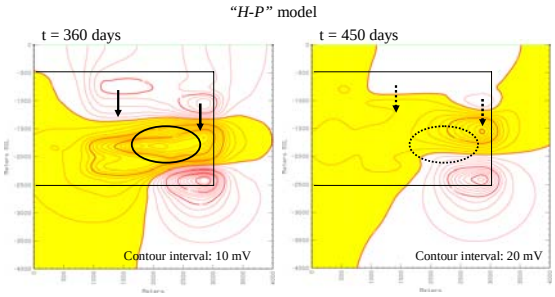

Figure 7: Cross-section of electric potential distribution under exploitation conditions for the *"H-P"* model. A three-month shut-in takes place from t = 360 to t = 450 days. Ellipse: production zone. Arrows: drag current associated with the liquid-phase downflow in the boiling zone.

In the case of the *"L"* models, the production zone is not overlain by the boiling zone and the influence of the positive potential can be transferred to the ground surface in the presence of a boundary separating regions of smaller (shallower) and larger (deeper) streaming potential coefficient magnitudes, which is associated with the vertical temperature gradient (see e.g., Ishido and Pritchett, 1999). The change in the SP distribution due to fluid production is caused by a combination of this positive source and the downward drag current in the deep boiling zone (Figure 8). In the *"L-F"* model, SP actually decreases during shut-in as shown in Figure 5. This is because of rapid disappearance of the positive source and sustained downward liquid flow through the matrix region.

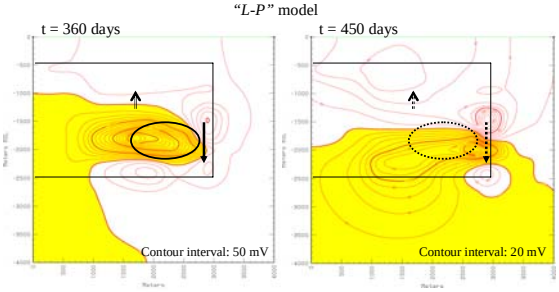

Figure 8: Cross-section of electric potential distribution under exploitation conditions for the *"L-P"* model. A three-month shut-in takes place from t = 360 to t = 450 days. Ellipse: production zone. Downward arrow: drag current associated with the liquid-phase downflow in the boiling zone. Upward arrow: dipole current source of "total potential" (see e.g., Ishido and Pritchett, 1999) due to pressure decrease, which appears at a boundary between regions of different streaming potential coefficient.

2.1.3 Reservoir Monitoring Using Gravity and SP Measurements Simultaneously

If the above four models were candidates to represent a real reservoir, what kinds of data would be useful to choose the best model among them? Temperature distribution data under natural-state conditions (from a number of wells) and pressure histories during exploitation conditions (from observation wells) would be helpful to distinguish the *"H"* and *"L"* models. Although production wellhead enthalpy histories are often valuable to distinguish *"P"* and *"F"* models, this is effective only for the *"L"* models in the present case (since only the *"L-F"* model exhibits "excess enthalpy" as mentioned above).

As seen in Figure 5, the histories of gravity and of self-potential at the earth surface are quite different among the four models. *"H-P"* can be distinguished from other three models based on long-term gravity changes. If long-term SP change data are available in addition to gravity changes, *"H-F"* can be distinguished from the others. Although both of the *"L"* models have very similar long-term gravity and SP trends, the short-term SP responses of the *"L-P"* and *"L-F"* models to shut-in are quite different. Since it is possible to measure long-term gravity changes with accuracy better than ~20 μGal using present-day repeat-survey technology (e.g., Sugihara, 2002) and to detect short-term SP changes within ~5 mV accuracy without sacrificing the low-cost advantages of SP techniques, a combination of long-term repeat gravity surveying and short-term continuous SP monitoring is believed to be a promising way to provide useful additional constraints in history-matching studies.

2.2 Illustrative Case II: High k Reservoir Associated with Major Fault

2.2.1 Reservoir Model

The reservoir model used here is essentially the same as the conceptual model for numerical studies of the natural evolution of a two-phase geothermal reservoir which has formed along the Ginyu fault in the Ogiri thermal area, Kyushu Island, Japan (Yano and Ishido, 1995). The model represented by the two-dimensional vertical cross-section shown in Figure 9 incorporates many of the major structural features of the Ginyu reservoir. The high-permeability reservoir (*A* in Fig. 9) is overlain by the low-permeability altered caprock (*C*). The model incorporates a 50-meter-wide permeable flow path (*F*) between the reservoir and the ground surface. Hot recharge water at temperature T_0 is assumed to enter the reservoir from below through a permeable conduit (*E*) at a mass flow rate M_0. A permeable horizontal conduit (*H*) allows for lateral mass outflow. The rocks *S* and *B* surrounding the reservoir are more permeable than the caprock, but the permeability of rock *B* is low enough that conduction is the dominant mode of heat transfer. The hot recharge water boils as it rises through the system. In the upper part of the reservoir, a portion of this fluid dries completely to pure steam, which then flows to the surface through the fracture in the caprock. The rest of the hot water leaves the reservoir to the west through the horizontal conduit *H*. Substantial fluid flows also take place in the shallow formation *S* above the caprock due to topographic effects.

All rock formations are assumed to be porous media; their properties range from 0.01 to 0.1 in porosity and from 0.01 mdarcy (for *C*) to 100 mdarcy (for *A*, *E* and *H*) in permeability. The two-dimensional computational grid shown in Figure 9 has the thickness of 250 m (in the north-south direction). All exterior boundaries except the top surface and a part of the western vertical surface, where the horizontal conduit intersects, are closed; pressure and temperature are maintained at 1 bar and 20 °C respectively along the top boundary, and the pressure at sea level along the western boundary is maintained at 40 bars. Any "*fresh water*" which flows downward into the grid through the top surface contains a dilute tracer to permit its identification.

A source of high-temperature "*magmatic water*" (similarly tagged with a dilute tracer) was imposed at the bottom of deep conduit (T_0=260 °C, M_0=36 kg/s); the evolution of the hydrothermal convection system was then simulated using the STAR geothermal simulator. The system reached quasi-steady state after around 5000 years; in Figure 9, the distributions of temperature, vapor saturation and fluid mass flux are shown for 6000 years.

The STAR simulator was also used to perform a 10-year forecast of the consequences of production and injection, starting from the natural-state model described above as the initial conditions. All boundary conditions and rock properties were the same as used to calculate the natural-state. Three hypothetical production wells and two injection wells were incorporated within the model. A constant total wellhead steam flowrate (sufficient to generate 20 MW of electricity) was assumed to be withdrawn from the

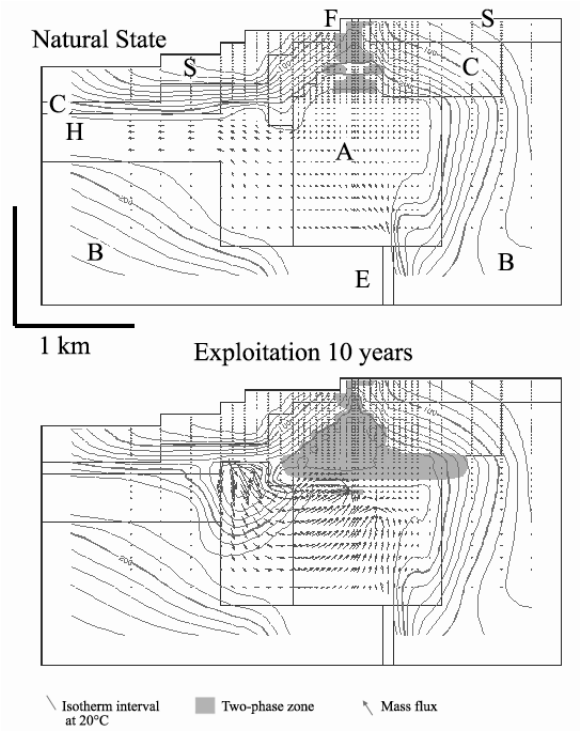

Figure 9: Two-dimensional reservoir model for Case II. Geological structure shown in upper frame. Temperature, mass flux and two-phase region shown under natural (upper) and exploited (lower) conditions. The grid extends vertically from -1550 m RSL to +850 m RSL.

production wells. A fixed separator pressure of 2.5 bars was used, and all separated liquid water (together with a small amount of steam condensate) was reinjected. (Although the present reservoir model roughly reproduces the natural-state features of the Ginyu reservoir, the locations of the various wells and the fluid production rate assumed in this calculation are all entirely hypothetical).

In Figure 9, the distributions of temperature, vapor saturation and fluid mass flux are shown after 10 years of field operation. The vapor zone expands about 400 m downward owing to the pressure decline caused by fluid production within the production area. The expansion of the vapor zone is quite rapid for the first couple of years of field operation, and thereafter becomes more gradual. (The

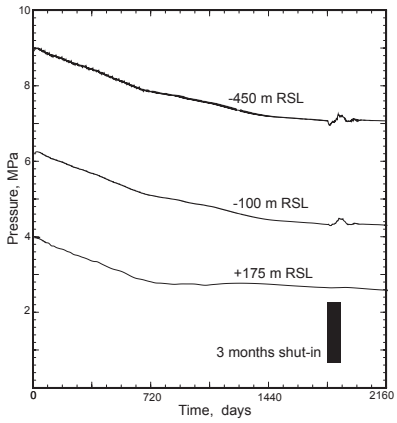

Figure 10: Pressure histories in three observation wells.

total volume occupied by steam increases from ~1x10^6 m^3 under natural-state condition to ~5x10^6 and ~6.5x10^6 m^3 after two and four years respectively.) The temporal variations of reservoir pressure and vapor phase saturation are shown for the first ~6 years of exploitation in Figures 10 and 11 respectively. In the calculation, the field is shut-in for three months after ~5 years of operation.

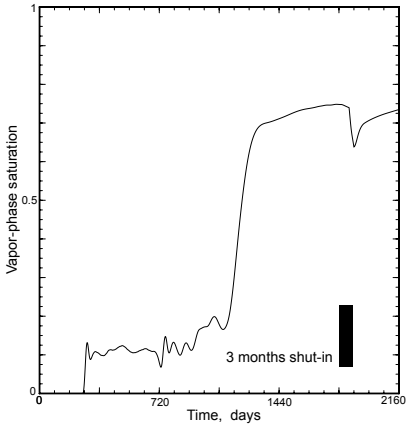

Figure 11: Change in vapor-phase saturation at a point located +100 mRSL in the upper part of the reservoir.

2.2.2 Change in Gravity

The microgravity postprocessor was applied to forecast gravity changes induced by the fluid production/reinjection operations based on the exploitation model described above. Large gravity disturbances are confined to the general vicinity of the production wells. As shown in Figure 12, gravity declines in the production area due to steam volume increase, approaching 60 μGal reduction in two years of production. In contrast, gravity change is small in the reinjection area. This is brought about by a combination of smaller decrease due to larger distance from the boiling zone and a slight increase due to cooling and fluid densification around the injection wells. Detectable signals should appear near the production wells during the first few years of field operation. In contrast to the results of Case I (Figure 5), gravity recovers ~5 μGal corresponding to the three months shut-in.

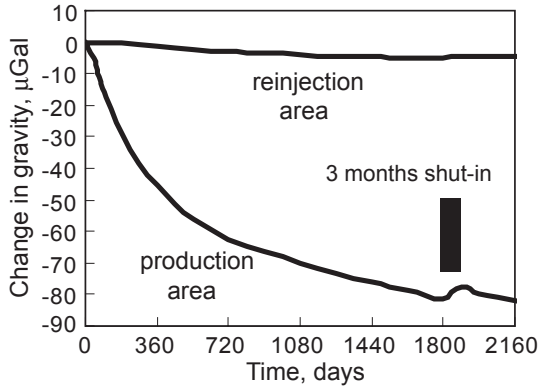

Figure 12: Changes in gravity in production and reinjection areas.

2.2.3 Change in Self-Potential

The EKP postprocessor was next applied to calculate SP changes induced by exploitation operation. For the self-potential calculations, the magmatic fluid is assumed to contain NaCl; the concentrations are proportional to the mass fraction of magmatic dilute tracer, and NaCl is 0.02 mol/l in the pure upflowing magmatic fluid entering from below. The fresh water is assumed to contain dilute NaCl (0.002 mol/l).

Within the portion of the SP-grid overlapped by the RSV-grid, the distribution of electrical conductivity is obtained directly from RSV-grid values. Elsewhere within the SP-grid, the electrical conductivity is assumed to be 0.01 S/m except in the region which is located at depths corresponding to the caprock region in the RSV-grid and 1 km in thickness in the north-south direction (where 0.1 S/m is assumed).

Figure 13 shows temporal changes in self-potential at two stations. The potential in the reinjection area decreases rapidly during the first a few months of field operation. This decrease in SP of more than 60 mV is associated with conduction-current sinks produced by pressure increase around the feedpoints of the reinjection wells. If this pressure change is localized at depth, the electrical potential change is limited to the region of pressure change in case of homogeneous C (streaming potential coefficient) (Ishido, 1989). However, in the present case, although the region of pressure increase is confined below the caprock, it contacts zero-C medium, caprock (assumed to be zero-C) at the upper side. So, the conduction current can be produced on the ground surface. The response to the three-months shut-in of all reinjection (and production) wells is striking in the reinjection area corresponding to the rapid pressure drawdown.

As shown in Figure 13, SP in the central production area decreases slightly (~20 mV) during the first three months of field operation, then begins to increase and becomes stable after about two years. In the production area, substantial production-induced expansion of the vapor-dominated zone takes place during the early stages of field operation. Just below the vapor zone, vigorous boiling occurs and counterflows of vapor (upward) and liquid (downward) are produced. This downward flow of the liquid phase carries electric (drag) current with it and brings about a negative SP change on the ground surface. This decrease in potential ceases in a relatively short time (about one year) in the present case.

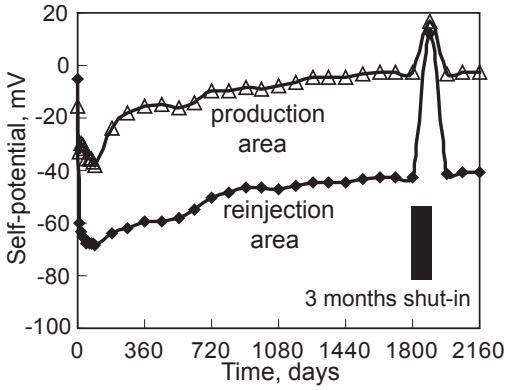

Figure 13: Changes in self-potential in production and reinjection areas.

In the production area, SP increase due to conduction current sources associated with the production wells is not so obvious. This is because the effect of conduction current sinks around the reinjection wells is transferred to the production area and is not negligible compared to that of the conduction current sources. Corresponding to the three-months shut-in, SP in the production area increases; this is mainly due to the rapid disappearance of conduction current sinks associated with the shut-in of reinjection wells.

2.2.4 Change in Magnetic Field

To simulate magnetic fields, two additional steps are required for the EKP postprocessor calculations (Ishido and Pritchett, 2001). At first, the postprocessor calculates the magnetic field due to electrokinetic coupling by applying the Biot-Savart law to the distributions of drag current density and conduction current density within the SP-grid. In this third step, the bottom and vertical sides of the SP-grid normally have "Neumann" conditions imposed upon them, in contrast to "Dirichlet" conditions normally adopted in the potential calculations.

Next, changes in magnetic field due to temperature-dependent rock magnetization are calculated, based upon computed changes in the underground reservoir temperature distribution in the RSV-grid. The pertinent parameters are temperatures T_1 and T_2 (with $T_1 < T_2$) and rock magnetization per unit volume M for each block in the RSV-grid. The magnetization per unit volume is taken to be equal to M_0 so long as the temperature (T) is less than T_1 and equal to zero if T exceeds T_2. For intermediate temperatures, Magnetization = $M \times (1 - 3\eta^2 + 2\eta^3)$ (where $\eta = (T - T_1) / (T_2 - T_1)$). For geothermal reservoir rocks, typical values for M_0 are in the range 1 – 10 amperes per meter. T_1 is typically in the range 100°C – 300°C, with T_2 in the range 500°C – 600°C. (In the present calculations, reservoir rocks A and H were taken to have M = 3 A/m, T_1 = 100°C, and T_2 = 600°C.)

Although geomagnetic anomaly magnitudes caused by electrokinetic coupling are too small to be observed, more substantial changes occur due to temperature-dependent rock magnetization. As Figure 14 shows, the total intensity increases to the south and decreases to the north of the reinjection area. This is caused by cooling of the rock around the feedpoints of the reinjection wells. The difference between the total intensity at a point south of reinjection area ("*R-S*") and that at a point north of reinjection area ("*R-N*") increases 7 nT and 20 nT during the first two and ten years of field operation respectively (Figure 15). The change after ten years of field operation corresponds to the increase in the magnetic moment caused by temperature decreasing more than 100°C within a 0.05 km^3 volume in the reinjection zone. At a point southwest of the production area, the total intensity decreases during the first two years (Fig. 14 and curve "*P-WSW*" in Fig. 15). This corresponds to the decrease in the magnetic moment caused by heating of shallow reservoir rock by vapor upflow (due to vigorous production-induced boiling) during the early stages of exploitation.

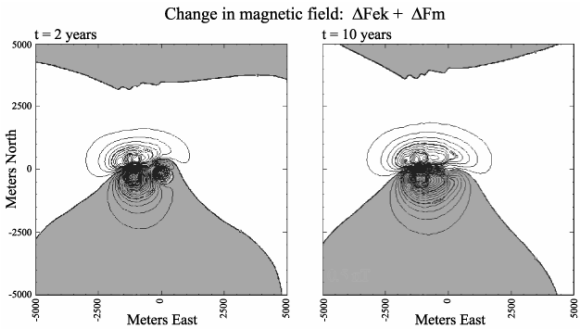

Figure 14: Horizontal contour maps of calculated change in total intensity after 2 and after 10 years of field operation. Area extends over –5 to +5 km E and –5 to +5 km N. Contour interval is 0.02 and 0.5 nT in the left and right plots respectively. Total intensity increases in shaded area.

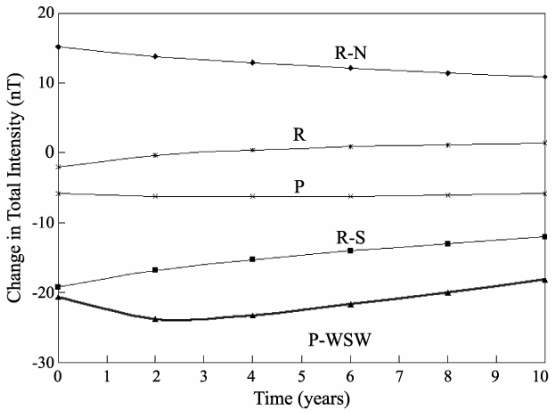

Figure 15: Total intensity variation with time. *"P"*: production area. *"R"*: reinjection area. *"R-N"* and *"R-S"*: station north and south of reinjection area respectively. *"P-WSW"*: station west-southwest of production area.

2.2.5 Change in Resistivity

Figure 16 shows changes in electrical conductivity (resistivity) near the production wells, which were calculated by using the EKP postprocessor. The electrical conductivity of the reservoir formation decreases from ~0.1 S/m to less than 0.01 S/m as the pore fluid boils from liquid to vapor. Such calculated "actual" resistivity changes can be used to appraise the utility of the various electrical survey techniques such as DC, MT and CSMT surveys.

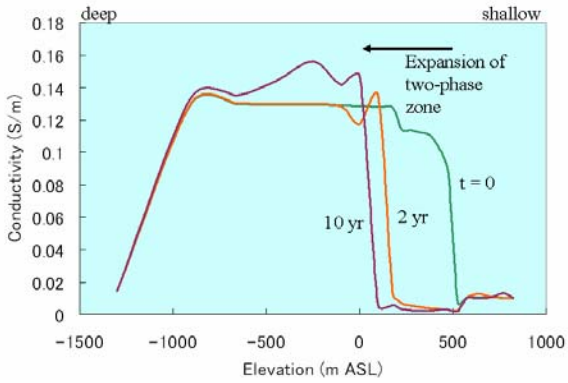

Figure 16: Changes in electrical conductivity in the production zone.

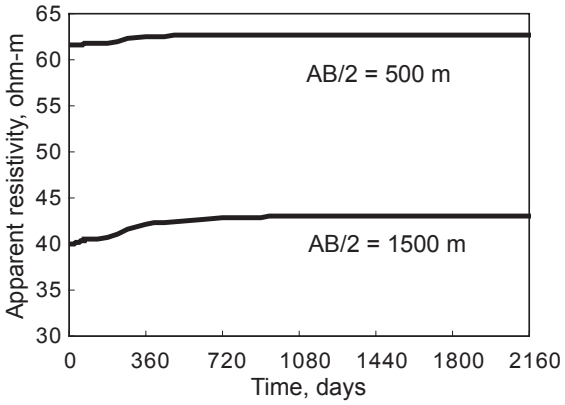

Figure 17: Changes in apparent resistivity for Schlumberger array extending in the north-south direction in the production area.

The DC resistivity postprocessor (see e.g., Pritchett, 2002) was applied to calculate changes in apparent resistivity for Schlumberger array. As shown in Figure 17, the apparent resistivity increases more than 5 % during the first two years of field operation for the array with 3000 m spacing between two current electrodes. This change reflects the increase in resistivity in the production area caused by the expansion of two-phase zone and reduction in liquid-phase saturation in the early stages of field operation.

2.2.6 Combination of Various Techniques

As shown in Figure 12, gravity declines substantially centered at the production area with steam volume increase within the two-phase zone below the caprock. In contrast, an anomaly near the reinjection area is very small to be detected. It is noteworthy that gravity appears to be more sensitive to the production region, whereas SP is more responsible to the injection zone (Figure 13). In the production area, although the negative SP anomalies associated with the expansion of two-phase zone appear, they are minor and disappear in a relatively short time in the present "Case II" compared to the previous "Case I".

Among techniques other than gravity and SP measurements, repeat or continuous measurement of geomagnetic field is quite promising to detect changes in reservoir rock temperature, especially the cooling due to reinjection operation. Repeat DC-resistivity surveys also provide additional information. In the present case, it is useful to monitor the expansion of two-phase zone in the production area.

Since SP is sensitive to flow pattern changes, substantial changes in SP can be observed at times of field-wide flow rate change even if the period is as short as one month (especially in the reinjection area). In the present case, changes in gravity also appear during the shut-in of production wells; this short-term change is not so large but can be detected by using present-day advanced technology. Frequently-repeat gravity surveying and continuous SP monitoring at times of field-wide shut-in of production and reinjection wells are promising to obtain useful data for improvement of any mathematical reservoir model by history-matching.

3. OUTLINE OF FIELD EXPERIMENTS AT THE OKUAIZU AND OGIRI AREAS

Under the collaborative research program "*System Integration of Various Geophysical Measurements for Reservoir Monitoring*", we are using multiple geophysical survey techniques to monitor field-wide shut-ins (usually associated with regularly-scheduled power station maintenance) in the operating Okuaizu and Ogiri geothermal fields in Japan.

In the Okuaizu field, we carried out continuous and/or repeat surveying of gravity and SP from March through November 2002 in cooperation with OAG (Okuaizu Geothermal) and Tohoku-EPCO (Tohoku Electric Power). During this time, a field wide shut-in took place (in March-April). Monitoring resumed in early April 2004 and is ongoing. We are carrying out history-matching studies using these results, together with various reservoir engineering data (taken by OAG) and previous geophysical monitoring data (gravity by OAG/Tohoku-EPCO, 1994–1997; 1998–2002, gravity by NEDO and repeat SP by GSJ) (see Nishi et al., 2005).

In this section, we describe some of the results obtained at the Ogiri field.

3.1 Long-Term Changes in Self-Potential and Resistivity at Ogiri

NEDO carried out a SP survey of the Ogiri field in 1998. Comparing this result to that in 1987 (Ishido et al., 1990), decreases in SP were detected both in the production and reinjection areas. These changes are thought to be induced by the exploitation operation started in 1996. In addition to repeat surveys, continuous SP monitoring was carried out by NEDO from 1998 through 2001. Total number of Pb-$PbCl_2$ electrodes involved in the measurement was more than 50 (Figure 18). Changes in SP more than 20-30 mV were observed near the production and reinjection wells respectively. These results can be roughly reproduced in the prediction calculations described in the previous section (Case II).

GSJ repeated 3-D electrical surveys six times between 1999 and 2002 by using the electrodes for the SP monitoring (Figure 18) as "potential" electrodes (Takakura et al., 2003). In each survey "current" electrodes made of stainless-steal were installed at eleven points within the survey area and at a remote point ~3 km south of the area. The pole-dipole data were collected using "Syscal-R2" resistivity equipment. In addition to seasonal variations of shallow resistivity structure, changes in resistivity of the upper part of the reservoir were detected: increase near the reinjection wells, changes near the production wells, etc. (Figure 19). Increase in resistivity in the production zone observed between February and August 2001 is thought to be caused by a new production well, which started to produce geothermal fluid from the upper part of the reservoir in March 2001.

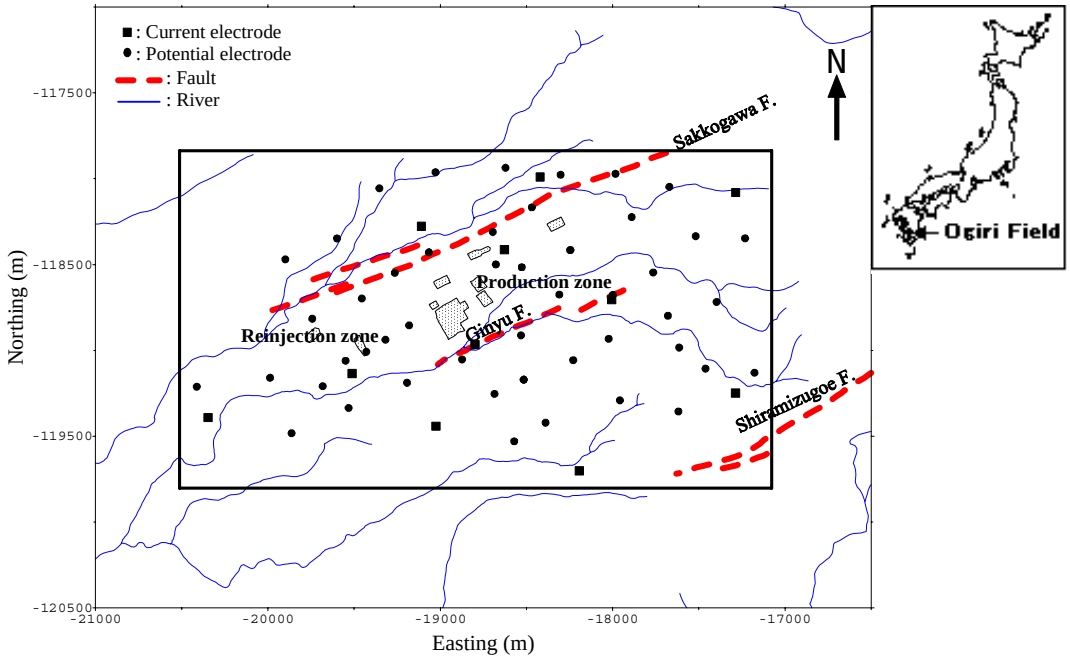

Figure 18: Location of electrodes used for continuous SP monitoring and repeat DC resistivity surveys at the Ogiri field.

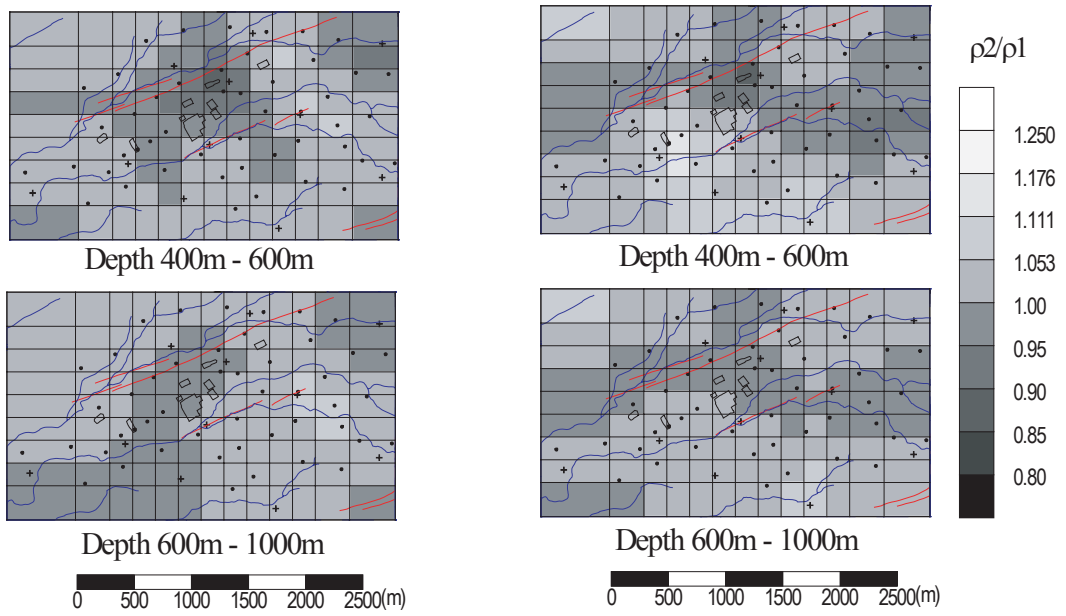

Figure 19: The ratio of resisitivity measured in February 2001 (left) and in August 2001 (right) to that measured in February 2000.

3.2 Short-Term Changes in Self-potential and Gravity at Ogiri

During the summer of 2002, various geophysical measurements (SP, gravity, GPS, tiltmeter and micro-earthquakes) were carried out in the Ogiri field.

Simultaneously, short-term production tests involving new exploratory wells drilled in the adjacent Shiramizugoe area (just south of Ogiri) were in progress. In collaboration with NKG (Nittetsu-Kagoshima Geothermal), monitoring resumed in early March 2003 and is ongoing. In April 2003, the production rate was substantially reduced for Ogiri power station maintenance. Short-term changes in SP and gravity (see Figure 20) were observed associated with this field-wide flow rate change. (As for the results of SP monitoring, see Tosha et al., 2005.)

We are carrying out history-matching studies using these data, supported by various reservoir engineering data (provided by NKG) and earlier SP results (a 1987 SP survey by GSJ/NEDO and 1998–2002 continuous/repeat SP measurements by NEDO).

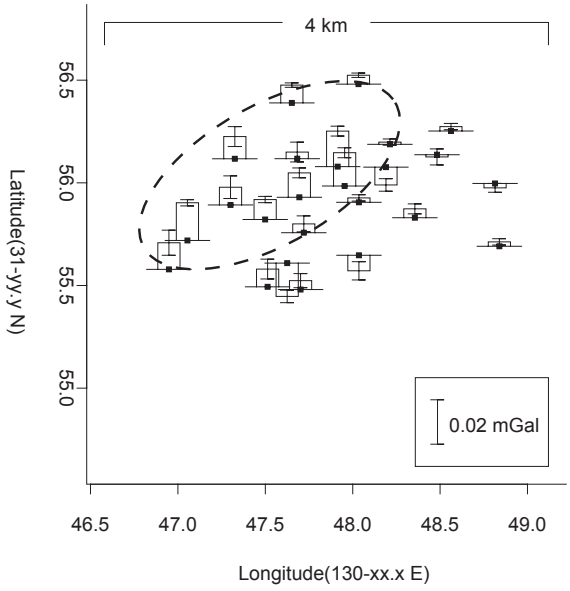

Figure 20: Changes in microgravity observed by "hybrid" measurements using relative and absolute gravimeters. Increases of more than 0.01 mGal were detected in the area denoted by ellipse associated with a field wide shut-in of production wells in April 2003 at Ogiri.

REFERENCES

Horikoshi, T., Yamasawa, S., Ide, T., and Tosha, T.: NEDO's Project on Development of Technology for Reservoir Mass and Heat Flow Characterization. (1) Project Outline and Techniques to Improve the Reservoir Model, Geothermal Resources Council *Transactions*, **25**, (2001), 641–644.

Ishido, T.: Self-Potential Generation by Subsurface Water flow Through Electrokinetic Coupling, *Detection of Subsurface Flow Phenomena*, Lecture Notes in Earth Sciences, Vol. 27, G.-P. Merkler et al. (Eds), Springer-Verlag, Berlin (1989), 121-131.

Ishido, T., Kikuchi, T., Yano, Y., Sugihara, M., and Nakao, S.: Hydrogeology Inferred from the Self-Potential Distribution, Kirishima Geothermal Field, Japan, Geothermal Resources Council *Transactions*, **14**-part II, (1990), 916-926.

Ishido, T., and Pritchett, J.W.: Numerical Simulation of Electrokinetic Potentials Associated with Subsurface Fluid Flow, *J. Geophys. Res.*, **104**, (1999), 15247–15259.

Ishido, T., and Pritchett, J.W.: Prediction of Magnetic Field Changes Induced by Geothermal Fluid Production and Reinjection, Geothermal Resources Council *Transactions*, **25**, (2001), 645-649.

Ishido, T. and Pritchett, J.W.: Characterization of Fractured Reservoirs Using Continuous Self-Potential Measurements, *Proceedings*, 28th Workshop on Geothermal Reservoir Engineering, Stanford University, Stanford, CA (2003).

Ishido, T., Sugihara, M., Pritchett, J.W., and Ariki, K.: Feasibility Study of Reservoir Monitoring Using Repeat Precision Gravity Measurements at the Sumikawa Geothermal Field, *Proceedings*, World Geothermal Congress 1995, Florence (1995).

Pritchett, J.W.: STAR: A Geothermal Reservoir Simulation System, *Proceedings*, World Geothermal Congress 1995, Florence (1995).

Pritchett, J.W.: *STAR's User Manual ver.9.0*, SAIC-02/1055, San Diego (2002).

Sugihara, M.: Precise Gravity Monitoring with a FG5 Absolute Gravimeter, at the Yanaizu-Nishiyama Geothermal Field, *Proceedings*, 24th New Zealand Geothermal Workshop, Auckland (2002).

Takakura, S., Sasaki, Y., Takahashi, T., and Takayama, J.: Repeated 3-D Electrical Surveys for Geothermal Reservoir Monitoring in the Ogiri Field, South Kyushu, Japan, *Proceedings*, 6th SEGJ International Symposium, Tokyo (2003).

Yamasawa, S., Tosha, T., Horikoshi, T., and Ide. T.: NEDO's Project on Development of Technology for Reservoir Mass and Heat Flow Characterization. (2) Geophysical Monitoring Techniques, Geothermal Resources Council *Transactions*, **25**, (2001), 701–704.

Yano, Y., and Ishido, T.: Numerical Modeling of the Evolution of Two-Phase Zones under a Fractured Caprock, *Geothermics*, **24**, (1995), 507-521.